Supplementary Material

Appendix

1 Opportunistic sighting records

Supplementary Table 1. Numbers of opportunistic sighting records contained in the eBird database through 2018 for four albatross species (SPP): Buller's (BUAL), Campbell (CAAL), grey-headed (GHAL), and white-capped (WCAL).

SPP	Sightings (n)	Date range
BUAL	5,087	1974-2018
CAAL	1,300	1972-2018
GHAL	1,901	1981-2018
WCAL	14,008	1973-2018

2 Geolocation Logging Sensor data

GLS tags record ambient light levels (solar irradiance) with respect to time and are often used to quantify animal movement. For processing GLS data, we used a zenith value of 96, removed light errors that were present in otherwise dark periods, and removed days in which locations could not be estimated. Movement parameters (alpha and beta) ranged from 0.1-0.2 and 0.1-0.7, respectively, depending on the properties of the track. Alpha is represents the distribution of time on the daylight side of each twilight you might expect the sensor to be obscured and beta represents the distribution of displacement (movement) from day to day.

A threshold value of 10 for luminescence at twilight was used except during brief periods when light appeared during the night. In such cases, the 'max_light_delta' function' within the 'twilightfree' package was used to find the max light in each 5 minute period and smoothed over every six observations. The threshold was recalculated based on the smoothed light values and the model was rerun until all erroneous light values were removed. Deployment and retrieval locations were also included in the model. Daily locations were estimated on either a 0.25 or 0.50 degree grid depending on the resolution of the track.

Supplementary Table 2. Summary of Geolocation Logging Sensor (GLS) data used in species distribution models to predict the probability of occurrence and habitat suitability for four species of albatross: Buller's (BUAL), white-capped (WCAL), grey-headed (GHAL), and Campbell (CAAL).

SPP	Deploymen t location	Tag model	Deployments / trips	Date range	Deployment days	
					Mean ± SDev	Range
BUAL	Snares Is	Mk5	32/36	2008-2011	408 ± 123	258-731
CAAL	Campbell Is	Mk7, Mk17	68/69	2009-2011	356 ± 53	274-729
GHAL	Campbell Is	Mk7, Mk17	62/103	2009-2013	586 ± 224	292-1106
WCAL	Auckland Is	Mk5	21/36	2006-2010	549 ± 245	236-1104

3 Description of environmental covariates

ETOPO-1, a 1 arc-minute global relief model of the earth's surface, and a high- resolution coastline, Global Self-consistent Hierarchical High-resolution Shorelines (GSHHS), were available and downloaded from the National Geophysical Data Canter (Wessel and Smith, 1996;

Amante and Eakins, 2009). Using the Euclidean distance tool in ArcGIS Pro version 2.4.1 (ESRI, 2019), we created a distance from land (DLAND) raster.

AVHRR pathfinder monthly sea surface temperature climatologies composed of data from 1985 to 2018 were available through the NOAA CoastWatch-West Coast Regional Node and Southwest Fisheries Science Center's Environment Research Division (Casey and Cornillon, 1999). Additionally, Modis-Aqua Level-3 binned monthly chlorophyll-*a* climatologies, comprised of data from 2002 to 2018, were downloaded from the Ocean Color website (NASA Goddard Space Flight Center et al., 2018). Global monthly sea surface temperature and chlorophyll-*a* climatologies were availible in 0.05° spatial resolution (~4.4 km) and were downloaded in netcdf format and converted to rasters in ArcGIS Pro.

Supplementary Table 3. Environmental variables used in species distribution models to predict the probability of occurrence and habitat suitability for four species of albatross: Buller's (BUAL), Campbell (CAAL), grey-headed (GHAL), and white-capped (WCAL).

Variable Abbreviation	Variable Name	Temporal Resolution	Unit	Description
DLAND	Distance from land	Static	m	Using GSSH for the coastline, distance from land was calculated using the spatial analysist extension in ArgGIS.
BATHY	Bathymetry	Static	m	Depth of the seafloor obtained from ETOPO-1, a one arc-minute global relief model of the earth's surface.
SST	Sea surface temperature	Monthly mean	°C	MODIS-Aqua SST product derived from Pathfinder SST. Climatologies provide a historically average value for SST on a 0.05 degree resolution from 1985 to 2018.
CHL	Chlorophyll-*a* concentration	Monthly mean	mg m^{-3}	A proxy for the amount of photosynthetic plankton, or phytoplankton, present in the ocean on a 0.05 degree global scale from 2002 to 2018.

4 Relative environmental suitability parameters

For the RES_{KERN} model, Min_P and Max_P values for each species were calculated by extracting environmental data for presences within each of the monthly 50% density contours created from the GLS data and taking the overall minimum and maximum values. Similarly, Min_A and Max_A were calculated by extracting monthly environmental data from the convex hull produced from the GLS data and taking the overall minimum and maximum values across months.

For the RES_{LIT} model, we estimated values for Min_A, Max_A, Min_P, and Max_P for DLAND, BATHY, SST, and CHL using habitat associations found in primary literature or from expert opinion for each seabird species. For variables in which little or no information was available in the literature, expert opinion was based on categories and definitions presented in Watson, Hiddink, Hobbs, Brereton & Tetley (2013) for BATHY, SST, and DLAND and Louzao et al (2006) for CHL.

Supplementary Table 4. Absolute and preferred minimum (Min_A, Min_P) and maximum (Max_A, Max_P,) values of bathymetric depth (m) (BATHY), distance from land (km) (DLAND), sea surface temperature (°C) (SST), and chlorophyll-a concentration (mg m^{-3}) (CHL) estimated from two sources: 1) monthly 50% kernel density contours, and 2) primary literature and/or expert opinion. Values from the two sources were used to inform Relative Environmental Suability models (RES_{KERN} and RES_{LIT}) for Buller's (BUAL), Campbell (CAAL), grey-headed (GHAL) and white-capped (WCAL) albatross.

SPP	MODEL	VARIABLE	Min_A	Max_A	Min_P	Max_P	Sources
BUAL	RES_{KERN}	DLAND	0.0	2706.7	0.0	1001.4	GLS
	RES_{KERN}	BATHY	0.4	9775.2	1.5	6428.1	GLS
	RES_{KERN}	SST	-2.9	28.1	-1.8	19.4	GLS
	RES_{KERN}	CHL	0.0	14.1	0.1	5.5	GLS
CAAL	RES_{KERN}	DLAND	0.0	2706.7	3.0	2623.5	GLS
	RES_{KERN}	BATHY	0.4	9775.2	1.5	6556.3	GLS
	RES_{KERN}	SST	-2.9	27.7	-1.5	19.7	GLS
	RES_{KERN}	CHL	0.0	21.9	0.1	2.2	GLS
GHAL	RES_{KERN}	DLAND	0.0	2706.7	0.0	2629.7	GLS
	RES_{KERN}	BATHY	0.4	9775.2	2.7	7487.3	GLS
	RES_{KERN}	SST	-2.9	25.7	-2.0	14.3	GLS
	RES_{KERN}	CHL	0.0	29.6	0.1	8.4	GLS
WCAL	RES_{KERN}	DLAND	0.0	1935.8	0.0	1201.4	GLS
	RES_{KERN}	BATHY	0.0	6280.4	1.3	6007.1	GLS
	RES_{KERN}	SST	-2.9	28.4	-2.9	20.6	GLS
	RES_{KERN}	CHL	0.0	11.5	0.1	7.5	GLS
BUAL	RES_{LIT}	DLAND	0.0	1000.0	5.0	300.0	(Sagar and Weimerskirch, 1996; Stahl et al., 1998; Stahl and Sagar, 2000a; b; 2006; Torres et al., 2013; Poupart et al., 2019)
	RES_{LIT}	BATHY	0.0	6000.0	100.0	4000.0	(Sagar and Weimerskirch, 1996; Stahl et al., 1998; Stahl and Sagar, 2000a; b; Spear et al., 2003; Stahl and Sagar, 2006; Torres et al., 2013; Poupart et al., 2019)
	RES_{LIT}	SST	8.0	22.0	10.0	20.0	(Poupart et al., 2019); expert opinion
	RES_{LIT}	CHL	0.1	4.0	0.8	3.2	(Poupart et al., 2019)
CAAL	RES_{LIT}	DLAND	0.0	3000.0	200.0	2000.0	(Waugh et al., 1999; Wakefield et al., 2011; Sztukowski et al., 2017; Sztukowski et al., 2018; Kroeger et al., 2019)
	RES_{LIT}	BATHY	0.0	6000.0	200.0	5000.0	(Waugh et al., 1999; Wakefield et al., 2011; Sztukowski et al., 2017; Sztukowski et al., 2018; Kroeger et al., 2019)
	RES_{LIT}	SST	0.0	24.0	2.0	18.0	(Waugh et al., 1999; Wakefield et al., 2011; Sztukowski et al., 2017; Sztukowski et al., 2018; Kroeger et al., 2019)

	RES_{LIT}	CHL	0.1	1.5	0.3	1.0	Expert opinion
GHAL	RES_{LIT}	DLAND	0.0	3000.0	750.0	2000.0	(Waugh et al., 1999; Cleeland et al., 2019; Kroeger et al., 2019)
	RES_{LIT}	BATHY	0.0	6000.0	2000.0	5000.0	(Waugh et al., 1999; Nel et al., 2001; Catry et al., 2004; Kroeger et al., 2019)
	RES_{LIT}	SST	0.0	15.0	5.0	9.0	(Waugh et al., 1999; Scales et al., 2016; Cleeland et al., 2019)
	RES_{LIT}	CHL	0.1	1.0	0.2	0.7	(Scales et al., 2016)
WCAL	RES_{LIT}	DLAND	0.0	1000.0	50.0	500.0	(Petersen et al., 2008; Torres et al., 2011)
	RES_{LIT}	BATHY	0.0	6000.0	200.0	4000.0	(Petersen et al., 2008; Torres et al., 2011)
	RES_{LIT}	SST	6.0	24.0	9.0	20.0	(Torres et al., 2011), expert opinion
	RES_{LIT}	CHL	0.1	1.0	0.2	0.4	Expert opinion

5 Boosted Regression Tree models

The learning rate determines the contribution of each successive tree to the final model as it proceeds through multiple iterations while the tree complexity allows for multiple interactions between variables. In this case, we used a tree complexity of three and learning rates that ranged between 0.005 and 0.100 for the BRT_{OS} models and 0.030 and 0.100 for the BRT_{GL} models. In addition, we used a bag fraction of 0.6 meaning that 60% of the data was randomly chosen as a training dataset for each iteration of the model fit. Initially 50 trees were fit using recursive partitioning of the data after which residuals for the initial fit were fit with another set of trees, and so forth, until the model deviance was minimized.

6 Opportunistic sighting records, geolocation tracks, and kernel density contours

6.1 Buller's albatross (*Thalassarche bulleri*)

Year-round GLS tracks for BUAL showed extensive transits between waters offshore the western coast of South America (extending from southern Chile to northern Peru) and the Tasman Sea (**Figure 1**). While the majority of opportunistic sightings overlapped the GLS tracks, several records were located further north, along the eastern coast of Australia, and one sighting was located in the central Indian Ocean (**Figure 1**). Monthly 50% data contours for the GLS data showed core areas located in waters off southern New Zealand from January to August and waters off the west coast of South America from June to January (**Figure 1**)

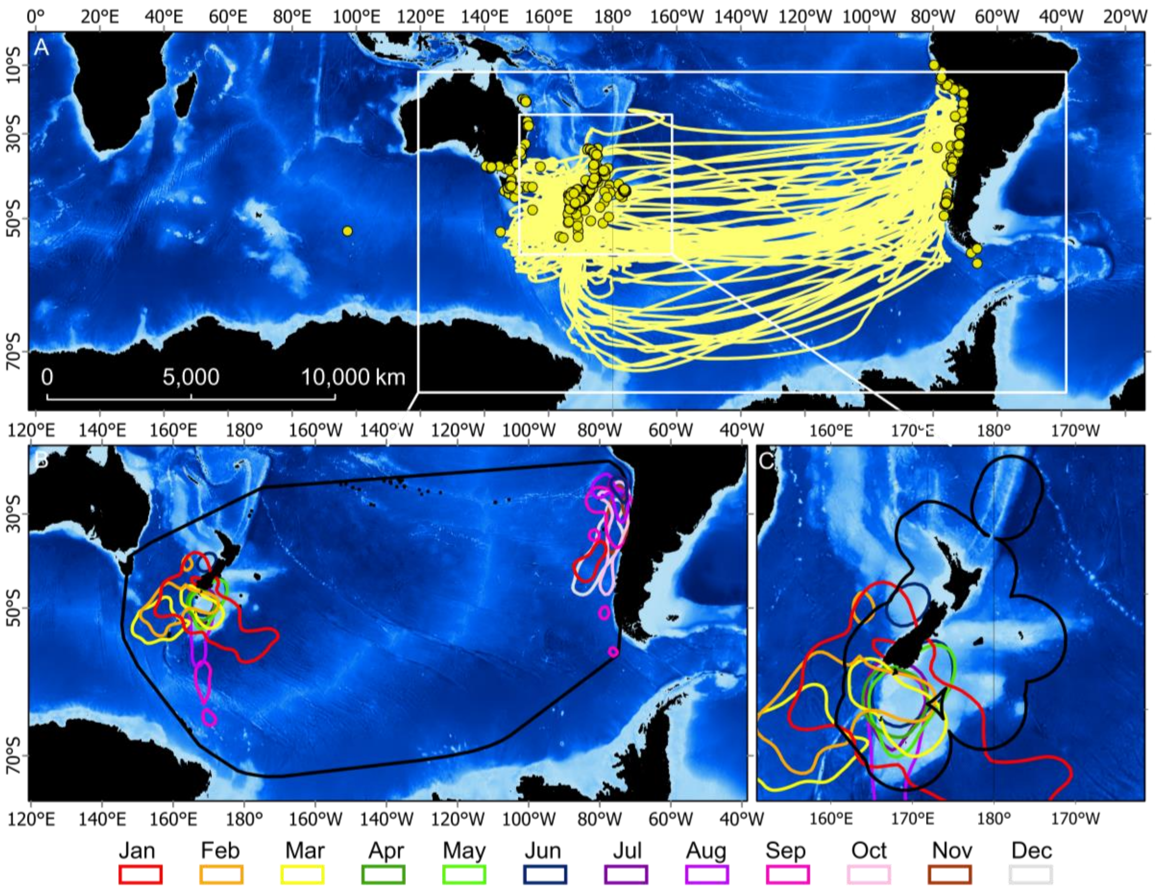

Supplementary Figure 1. Opportunistic sighting records (circles) and geolocation tracks (lines) for Buller's albatross (**A**) and minimum convex hull (black) with 50% kernel density contours color-coded by month generated from geolocation data (**B-C**).

6.2 Campbell albatross (*Thalassarche impavida*)

The majority of CAAL GLS tracks extended from the eastern Indian Ocean to offshore the southern and central coast of Chile and ranged from off the coast of Antarctic in the south to central Australia to the north (**Figure 2**). One CAAL failed in its breeding attempt relatively early in the breeding season, departed east wards from Campbell Island and circumnavigated the planet before returning to the colony in time for the breeding season the following year. All opportunistic sighting records were in good agreement with GLS data (**Figure 2**). Monthly 50% data contours showed core areas located in waters off southern NZ, beyond the EEZ, in January (**Figure 2**). From February to August, core areas spread to waters to the east of NZ and in the Great Australian Bight. Finally, between September and December core areas were located south of New Zealand (**Figure 2**).

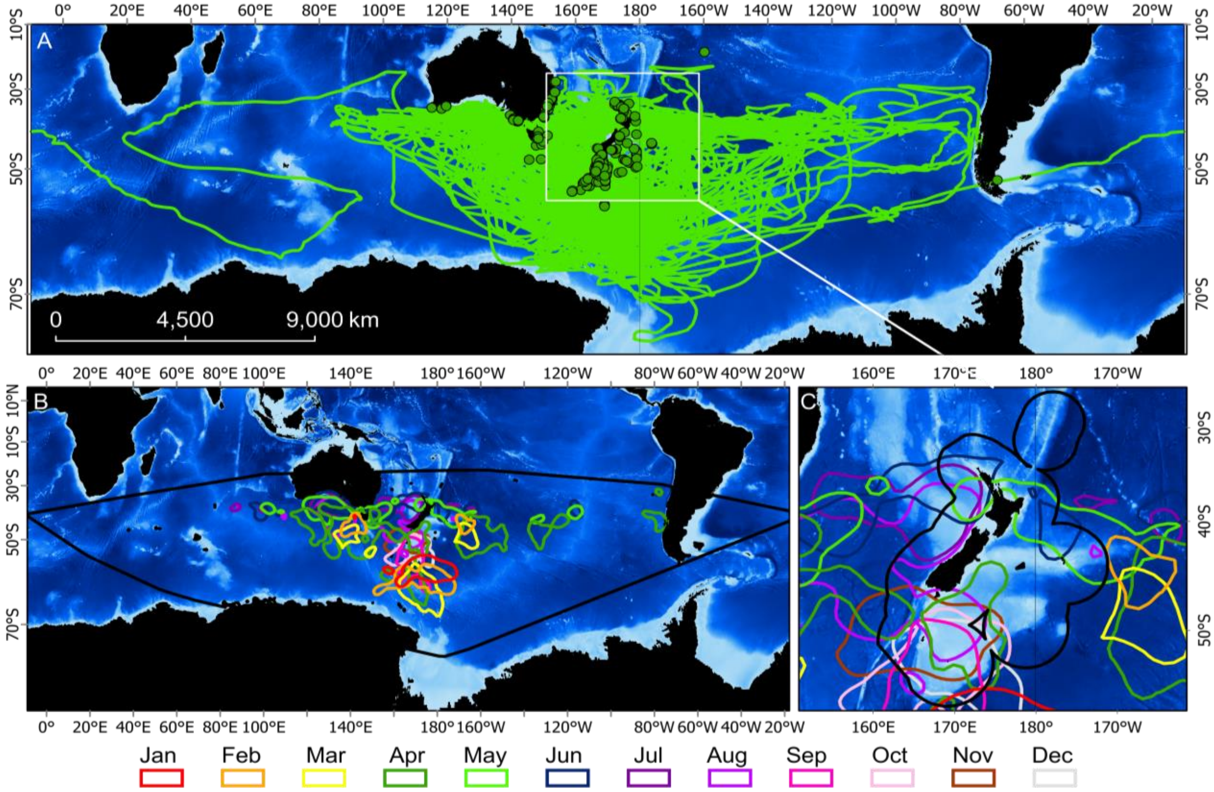

Supplementary Figure 2. Opportunistic sighting records (circles) and geolocation tracks (lines) for Campbell albatross (**A**) and minimum convex hull (black) with 50% kernel density contours color-coded by month generated from geolocation data (**B-C**).

6.3 Grey-headed albatross (*Thalassarche chrysostoma*)

Year-round GLS tracks for GHAL extended around the world between 30-75°S (**Figure 3**). Overall, opportunistic sighting records were in broad agreement with the GLS data, with some sightings extending further north. Sighting records were congregated in the Indian Ocean, the Tasman Sea and between the Antarctic Peninsula and the southern tip of South America (**Figure 3**). Of the 62 GHAL tracked, six birds circumnavigated the planet from east to west. Monthly 50% data contours showed core areas located in waters south-southeast of New Zealand, both inside and outside the EEZ, year-round (**Figure 3**). Core areas were also located in waters off the western coast of southern Chile from January to May and the Pacific Ocean in December and January (**Figure 3**). Core areas were located inside the southern portion of NZ's EEZ from July to January (**Figure 3**).

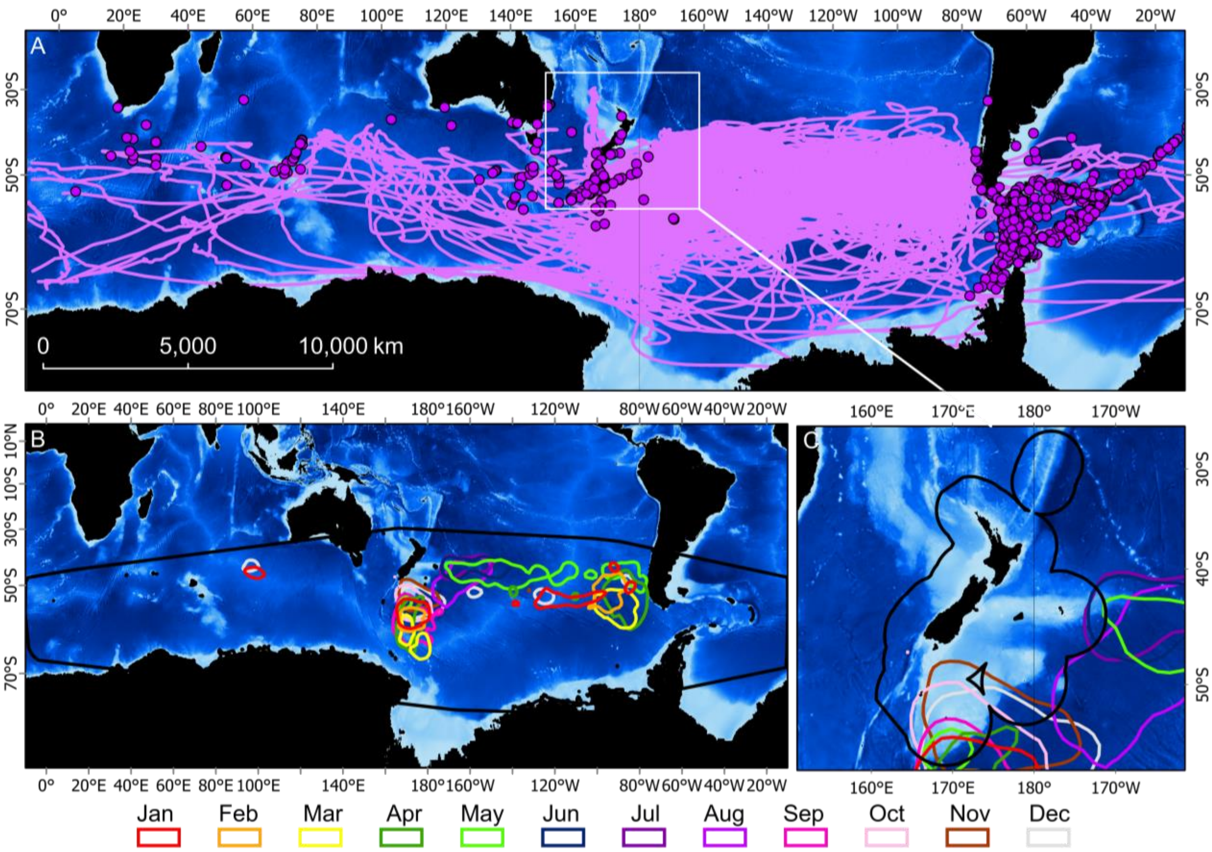

Supplementary Figure 3. Opportunistic sighting records (circles) and geolocation tracks (lines) for grey headed albatross (**A**) and minimum convex hull (black) with 50% kernel density contours color-coded by month generated from geolocation data (**B-C**).

6.4 White-capped albatross (*Thalassarche steadi*)

Year-round GLS tracks depicted WCAL traveling between the Tasman Sea and the South Atlantic and Southern Oceans, between Antarctica and southwestern Africa (**Figure 4**). Opportunistic sighting records were in general agreement with GLS data except for areas off the coast of South America. Core areas located in waters south-southwest of NZ, both within and beyond the EEZ, and in waters around Tasmania year-round (**Figure 4**). In select months, most notably November to January, core areas were located off the southwest coast of Africa (**Figure 4**).

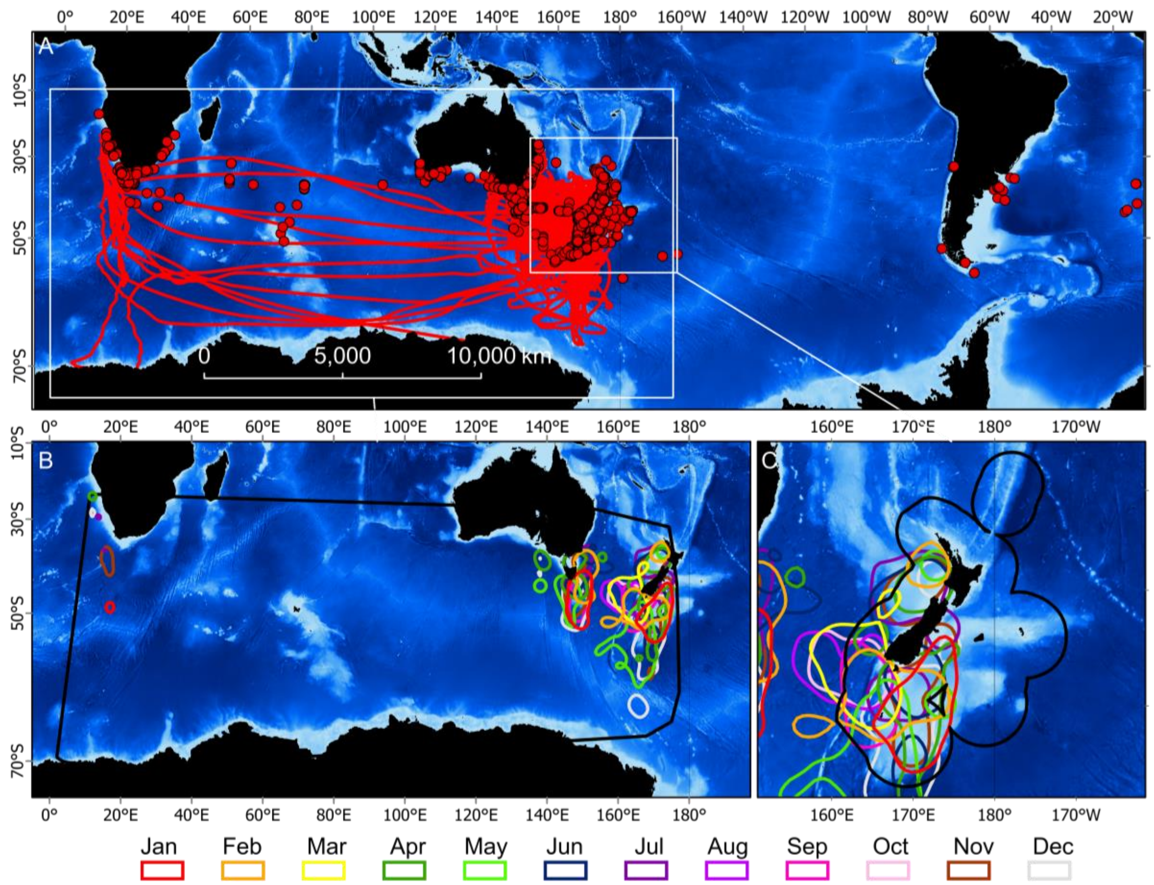

Supplementary Figure 4. Opportunistic sighting records (circles) and geolocation tracks (lines) for white-capped albatross (**A**) and minimum convex hull (black) with 50% kernel density contours color-coded by month generated from geolocation data (**B-C**).

7 Variable correlation matrixes

The following figures show the Pearson correlation matrix of environmental variables for opportunistic sighting and GLS data used to predict the probability of occurrence for each of four albatross species.

7.1 Buller's albatross

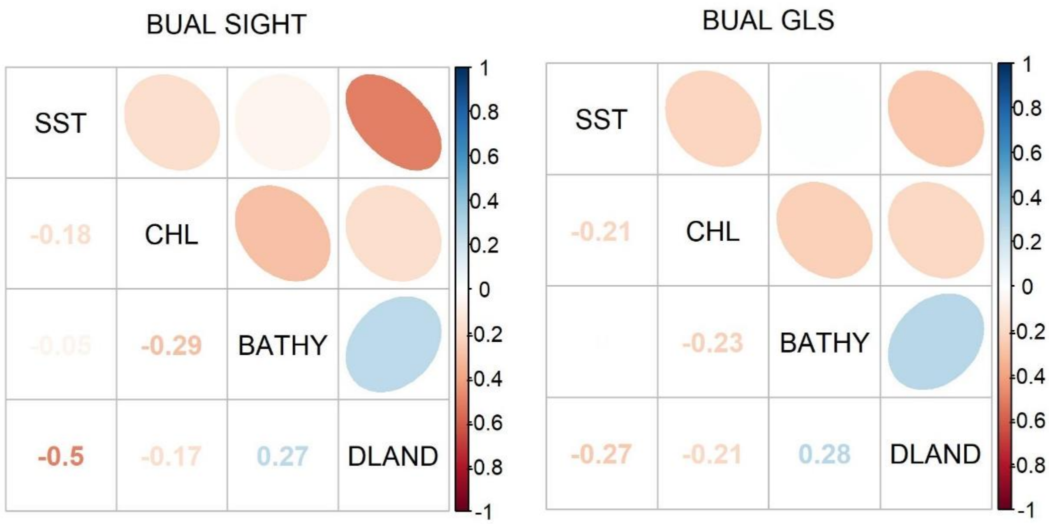

Supplementary Figure 5. Pearson correlation matrix of environmental variables used to predict the probability of Buller's albatross (BUAL) occurrence using opportunistic sightings (left) and geolocation data (right). Positive correlations are displayed in blue and negative correlations in red color. Color intensity, shape and orientation of the ellipse depend on the correlation value.

7.2 Campbell albatross

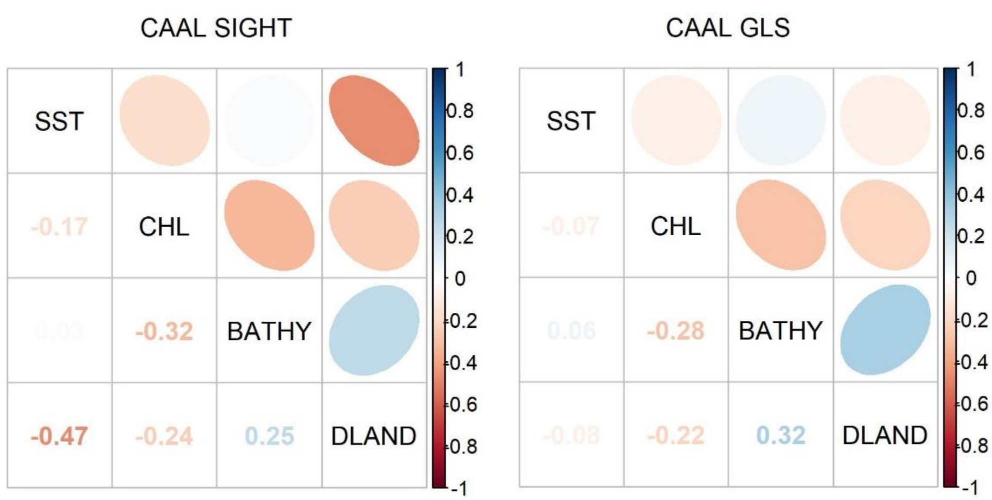

Supplementary Figure 6. Pearson correlation matrix of environmental variables used to predict the probability of Campbell albatross (CAAL) occurrence using opportunistic sightings (left) and geolocation data (right). Positive correlations are displayed in blue and negative correlations in red color. Color intensity, shape and orientation of the ellipse depend on the correlation value.

7.3 Grey-headed albatross

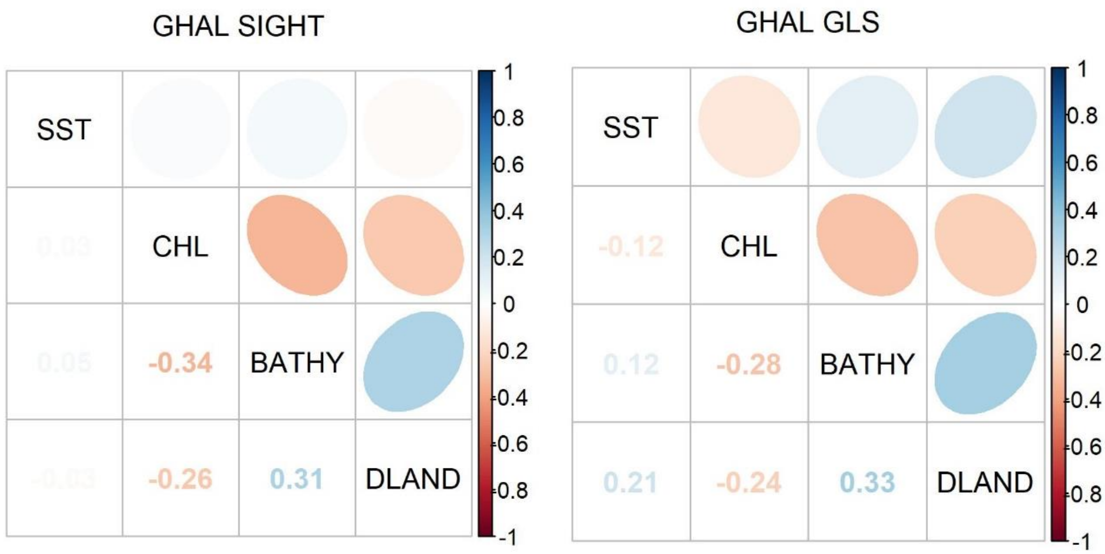

Supplementary Figure 7. Pearson correlation matrix of environmental variables used to predict the probability of grey-headed albatross (GHAL) occurrence using opportunistic sightings (left) and geolocation data (right). Positive correlations are displayed in blue and negative correlations in red color. Color intensity, shape and orientation of the ellipse depend on the correlation value.

7.4 White-capped albatross

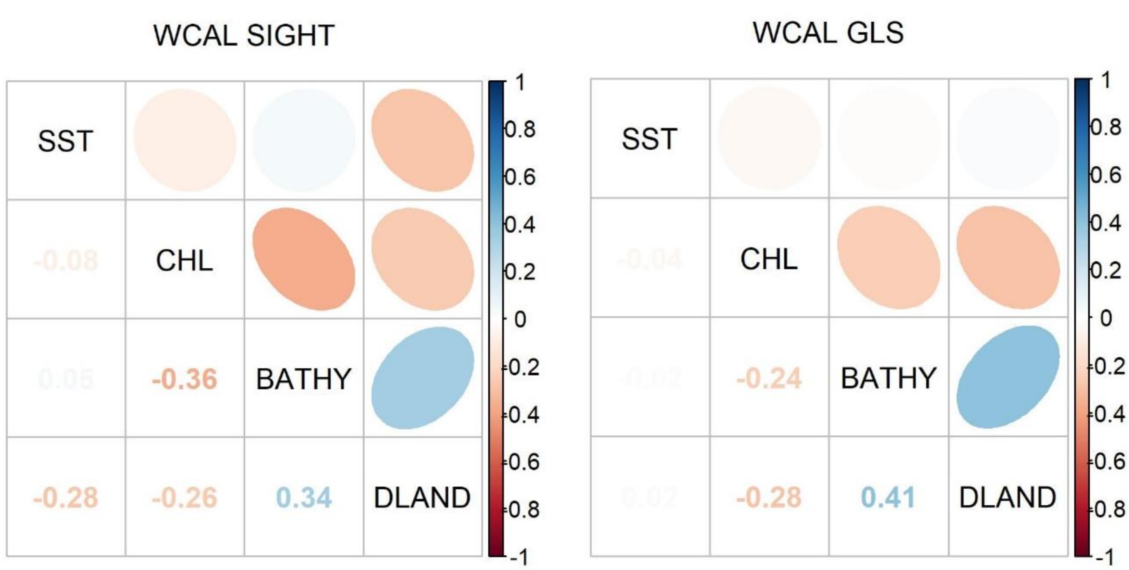

Supplementary Figure 8. Pearson correlation matrix of environmental variables used to predict the probability of white-capped albatross (WCAL) occurrence using opportunistic sightings (left) and geolocation data (right). Positive correlations are displayed in blue and negative correlations in red color. Color intensity, shape and orientation of the ellipse depend on the correlation value.

8 Relationship between occurrence and environmental variables

The following figures show the relationship between the probability of occurrence and four environmental predictor variables for two RES and two BRT models for each four albatross species.

8.1 Campbell albatross

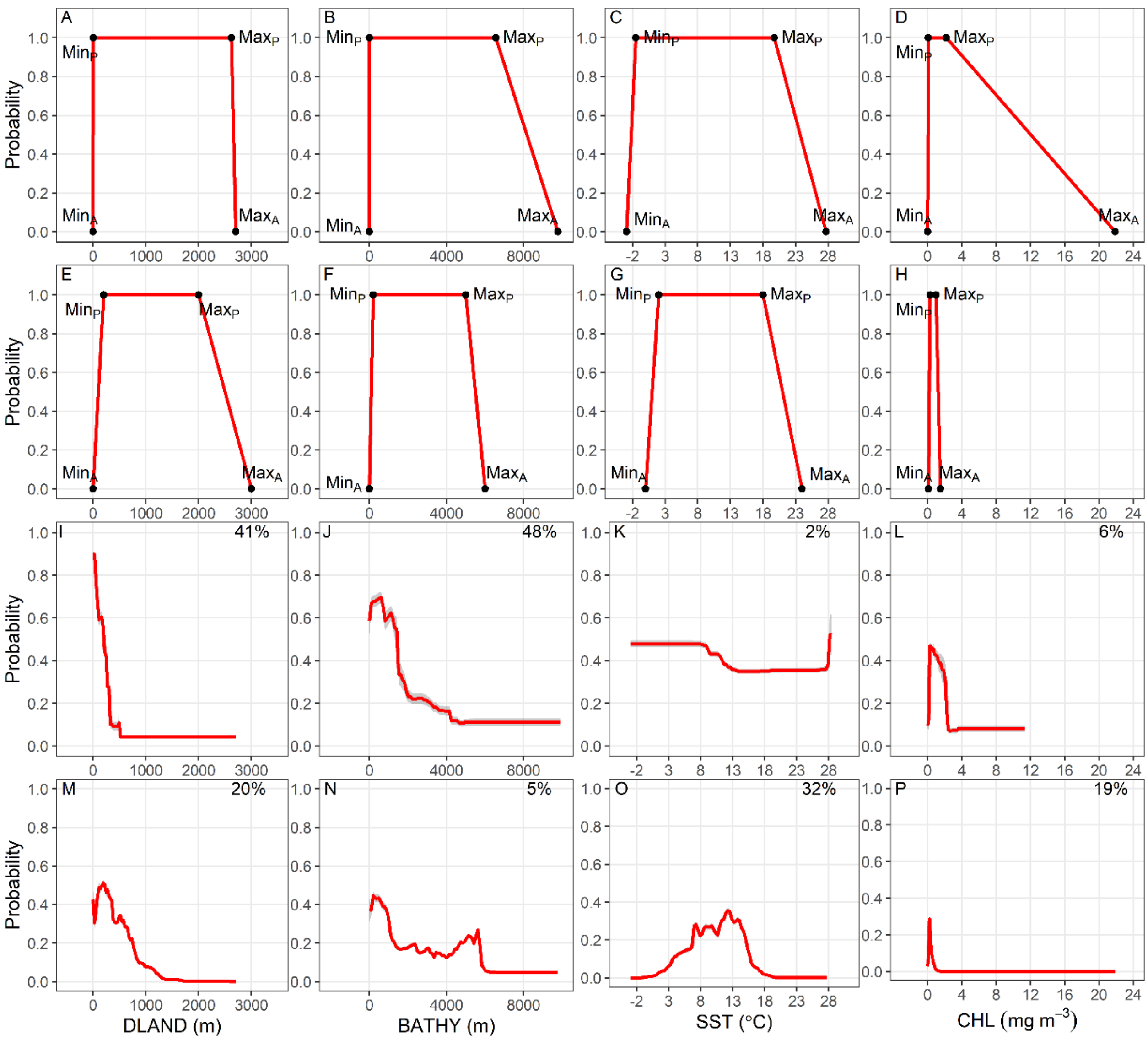

Supplementary Figure 9. Relationship between the probability of Campbell albatross occurrence and four environmental predictor variables: Bathymetry (BATHY), distance from land (DLAND), sea surface temperature (SST) and chlorophyll-a (CHL). Top two rows show trapezoidal response curves for each environmental variable used in two Relative Environmental Suitability models (one fit with values obtained from the monthly 50% kernel density contours from geolocation data and background environmental data (RES_{KERN}, **A-D**), and one fit with values from the literature and expert opinion (RES_{LIT}, **E-H**)). Minimum and maximum absolute and preferred habitat values are denoted by Min_A, Max_A, Min_P, and Max_P. Bottom two rows show partial dependence plots for each environmental variable from two bootstrapped Boosted Regression Tree models (one fit with opportunistic sightings data (BRT_{OS}, **I-L**), and one fit with geolocation data (BRT_{GL}, **M-P**)). Red lines represent response curves with grey shading showing the standard deviation. Percentage contribution for each variable is shown on the top right corner.

8.2 Grey-headed albatross

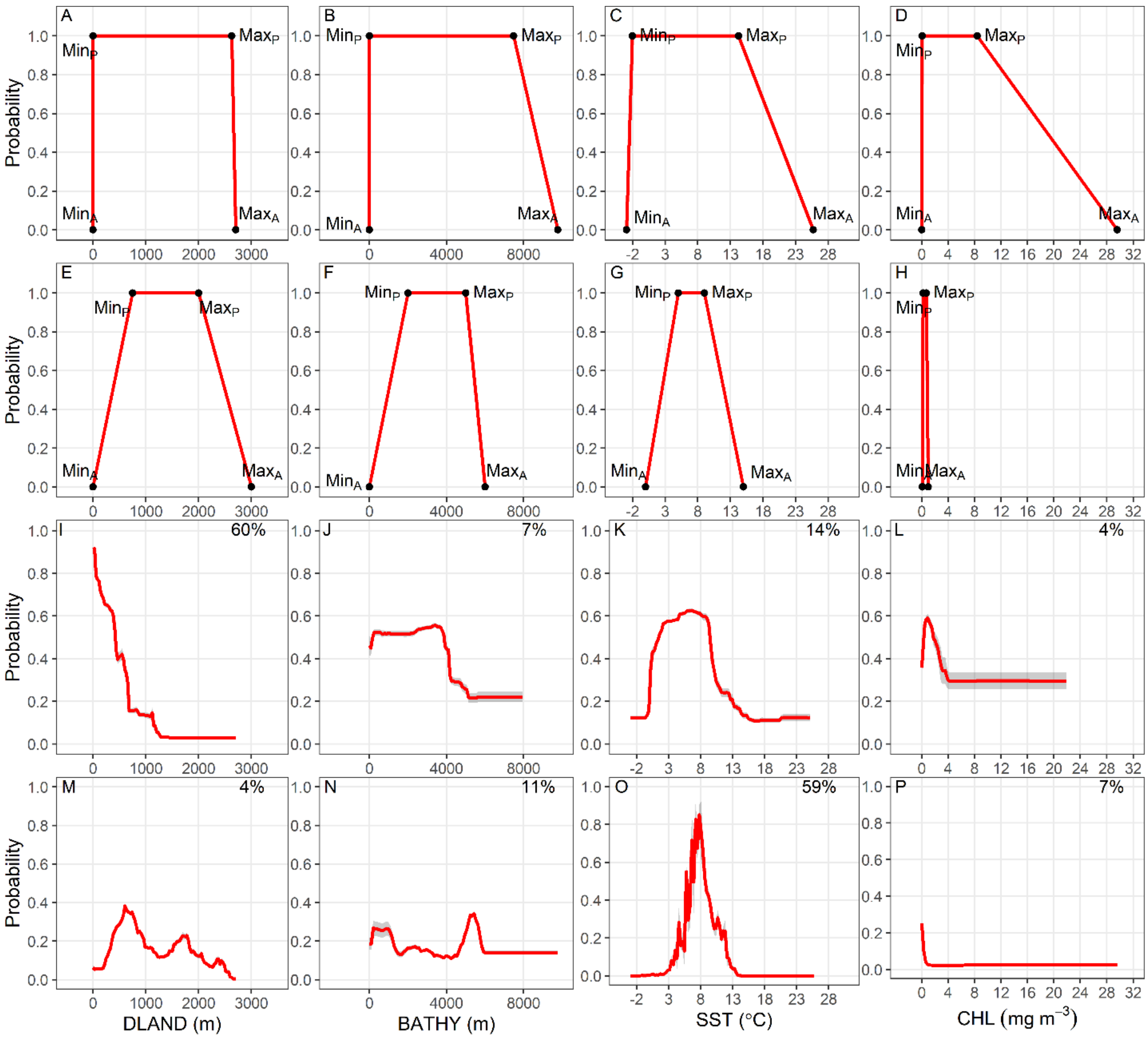

Supplementary Figure 10. Relationship between the probability of grey-headed albatross occurrence and four environmental variables: Bathymetry (BATHY), distance from land (DLAND), sea surface temperature (SST) and chlorophyll-a (CHL). Top two rows show trapezoidal response curves for each environmental variable used in two Relative Environmental Suitability models (one fit with values obtained from the monthly 50% kernel density contours from geolocation data and background environmental data (RES_{KERN}, **A-D**), and one fit with values from the literature and expert opinion (RES_{LIT}, **E-H**)). Minimum and maximum absolute and preferred habitat values are denoted by Min_A, Max_A, Min_P, and Max_P. Bottom two rows show partial dependence plots for each environmental variable from two bootstrapped Boosted Regression Tree models (one fit with opportunistic sightings data (BRT_{OS}, **I-L**), and one fit with geolocation data (BRT_{GL}, **M-P**)). Red lines represent response curves with grey shading showing the standard deviation. Percentage contribution for each variable is shown on the top right corner.

8.3 White-capped albatross

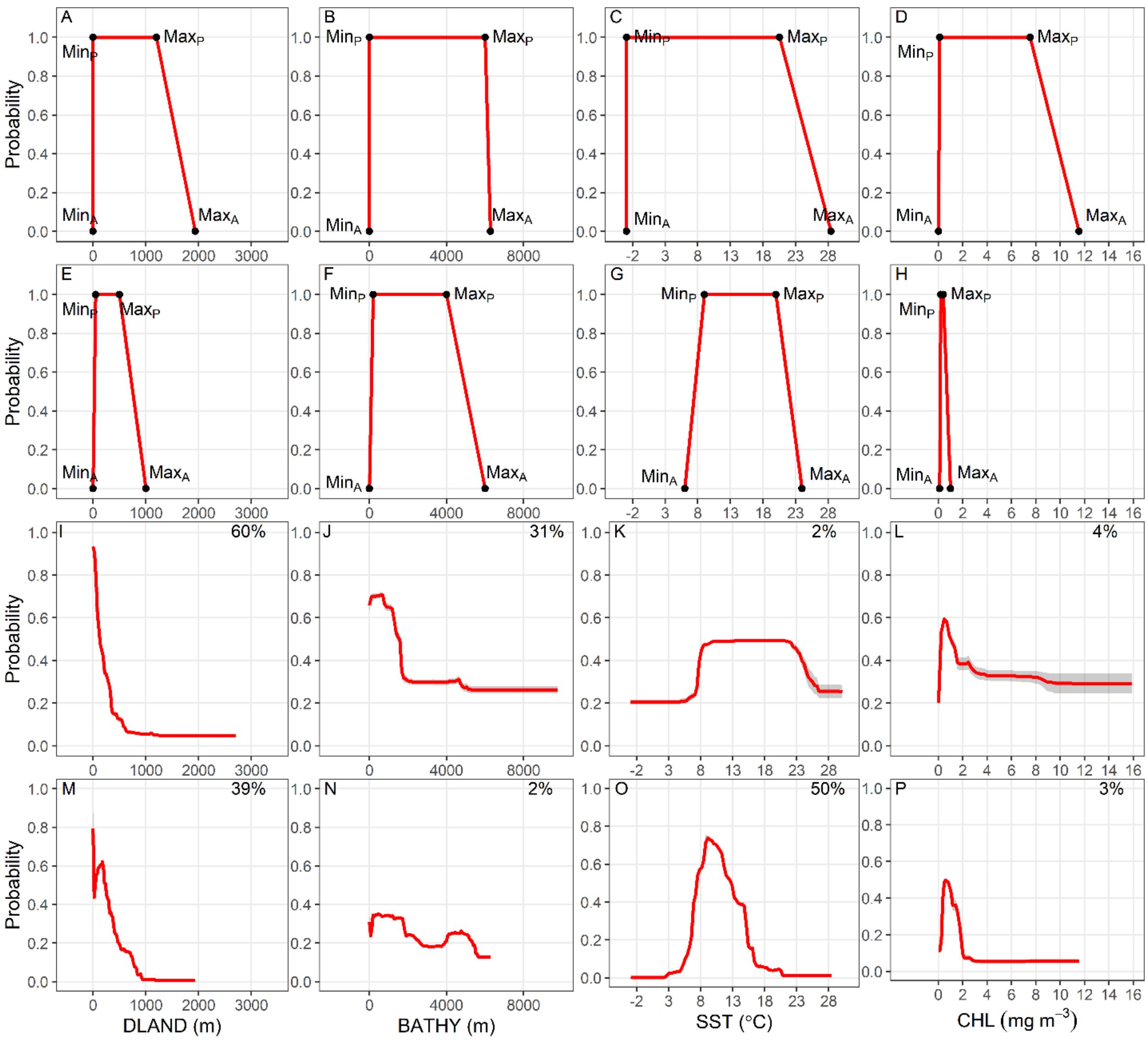

Supplementary Figure 11. Relationship between the probability of white-capped albatross occurrence and four environmental variables: Bathymetry (BATHY), distance from land (DLAND), sea surface temperature (SST) and chlorophyll-a (CHL). Top two rows show trapezoidal response curves for each environmental variable used in two Relative Environmental Suitability models (one fit with values obtained from the monthly 50% kernel density contours from geolocation data and background environmental data (RES_{KERN}, **A-D**), and one fit with values from the literature and expert opinion (RES_{LIT}, **E-H**)). Minimum and maximum absolute and preferred habitat values are denoted by Min_A, Max_A, Min_P, and Max_P. Bottom two rows show partial dependence plots for each environmental variable from two bootstrapped Boosted Regression Tree models (one fit with opportunistic sightings data (BRT_{OS}, **I-L**), and one fit with geolocation data (BRT_{GL}, **M-P**)). Red lines represent response curves with grey shading showing the standard deviation. Percentage contribution for each variable is shown on the top right corner.

9 Predicted probability of presence and habitat

The following figures show the predicted probability of presence and habitat predicted by two RES and two BRT models for each four albatross species.

9.1 Campbell albatross

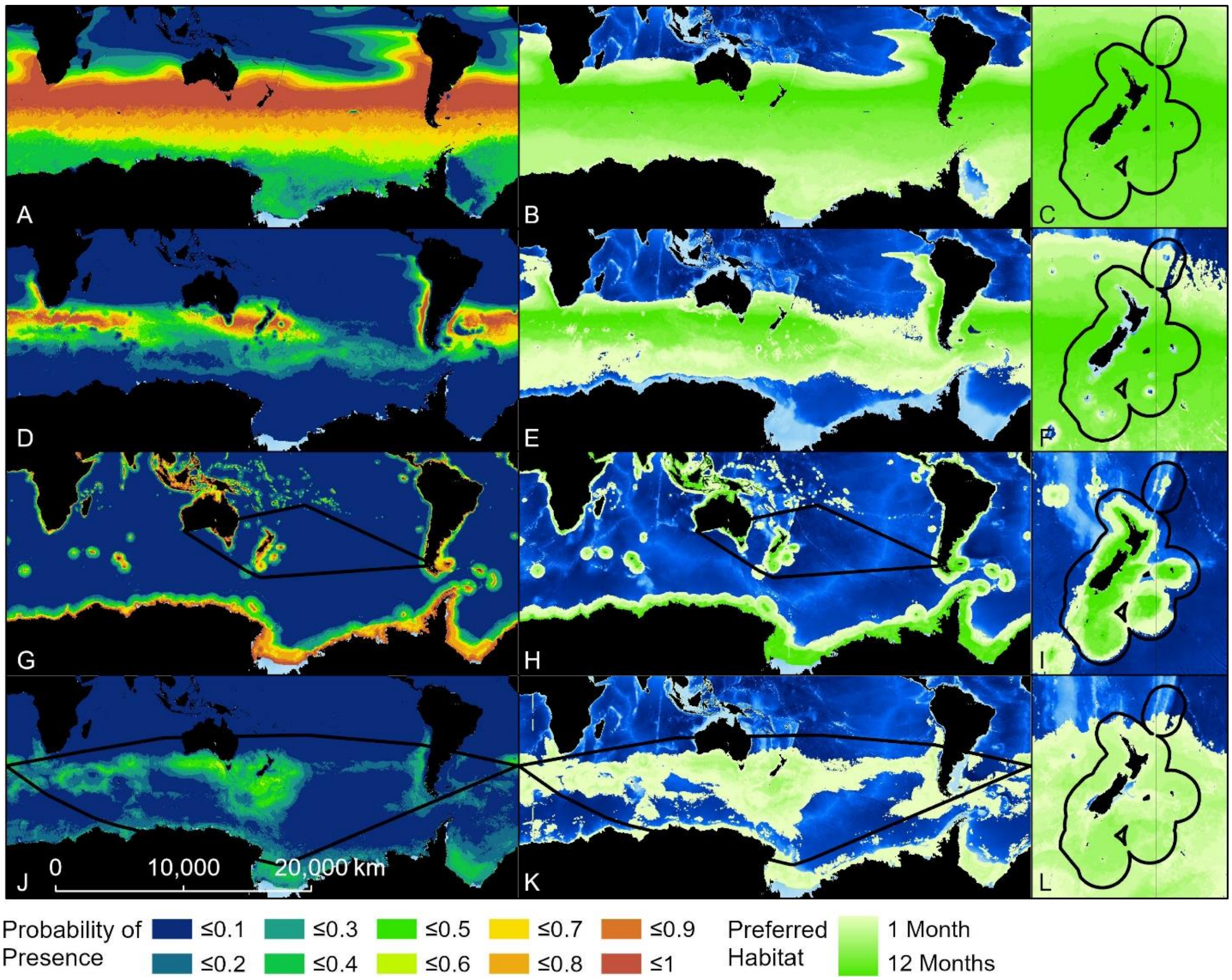

Supplementary Figure 12. Probability of presence and habitat of Campbell albatross predicted by four models. Top two rows show results from two Relative Environmental Suitability models (one fit with values obtained from the monthly 50% kernel density contours from geolocation data (RES_{KERN}, **A-C**), and one fit with values from the literature and expert opinion (RES_{LIT}, **D-**

F)). Bottom two rows show results from two Boosted Regression Tree models (one fit with opportunistic sightings data (BRT_{OS}, **G-I**), and one fit with geolocation data (BRT_{GL}, **J-L**)). Black boundaries indicate the minimum convex hull (**G, H, J, K**) or NZ Exclusive Economic Zone (**C, F, I, L**) and habitat is color-scaled from 1 to 12 indicating the number of months each cell was classified as habitat.

9.2 Grey-headed albatross

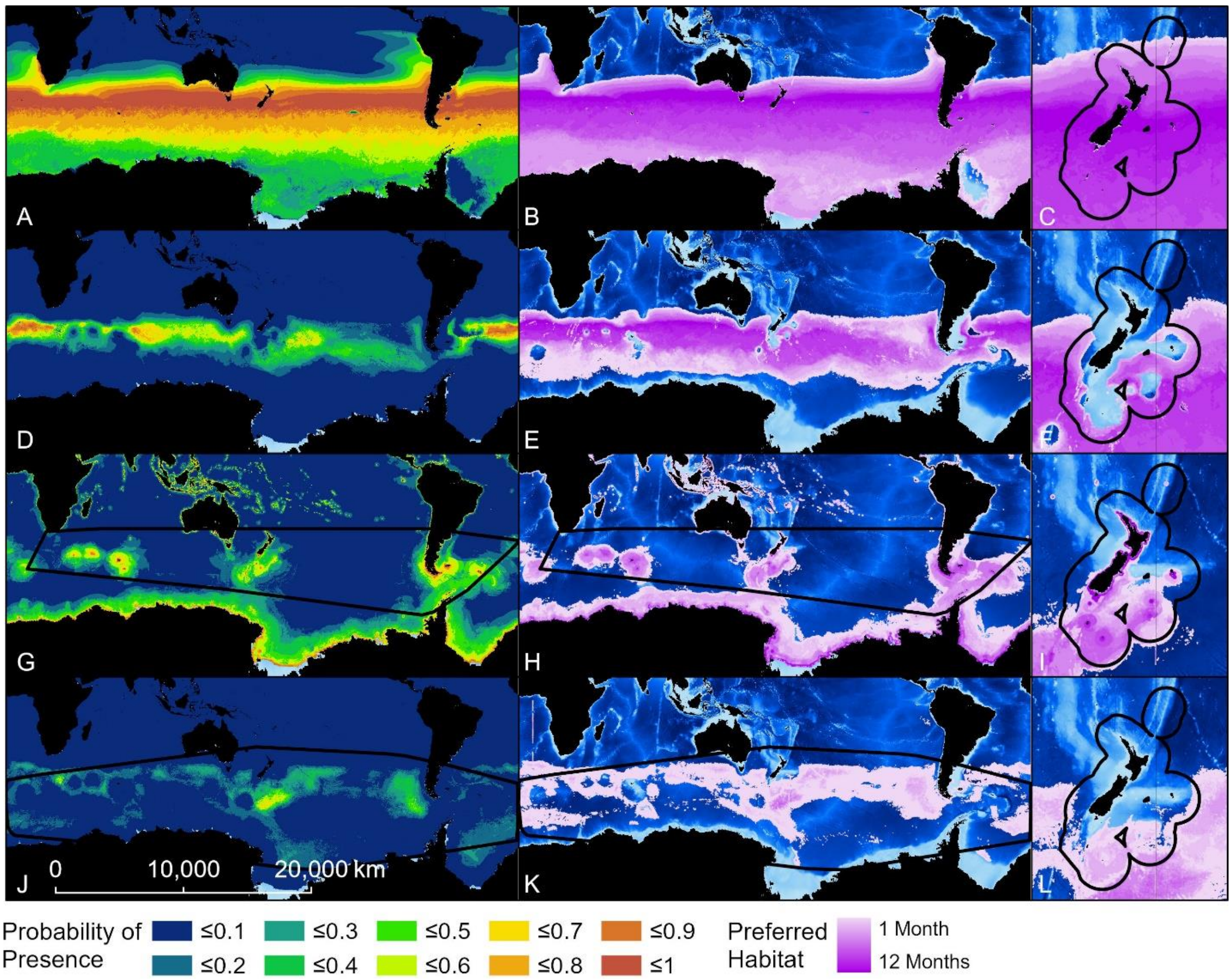

Supplementary Figure 13. Probability of presence and habitat of grey-headed albatross predicted by four models. Top two rows show results from two Relative Environmental Suitability models (one fit with values obtained from the monthly 50% kernel density contours from geolocation data (RES_{KERN}, **A-C**), and one fit with values from the literature and expert opinion (RES_{LIT}, **D-F**)). Bottom two rows show results from two Boosted Regression Tree models (one fit with opportunistic sightings data (BRT_{OS}, **G-I**), and one fit with geolocation data (BRT_{GL}, **J-L**)). Black boundaries indicate the minimum convex hull (**G, H, J, K**) or NZ Exclusive Economic Zone (**C, F, I, L**) and habitat is color-scaled from 1 to 12 indicating the number of months each cell was classified as habitat.

9.3 White-capped albatross

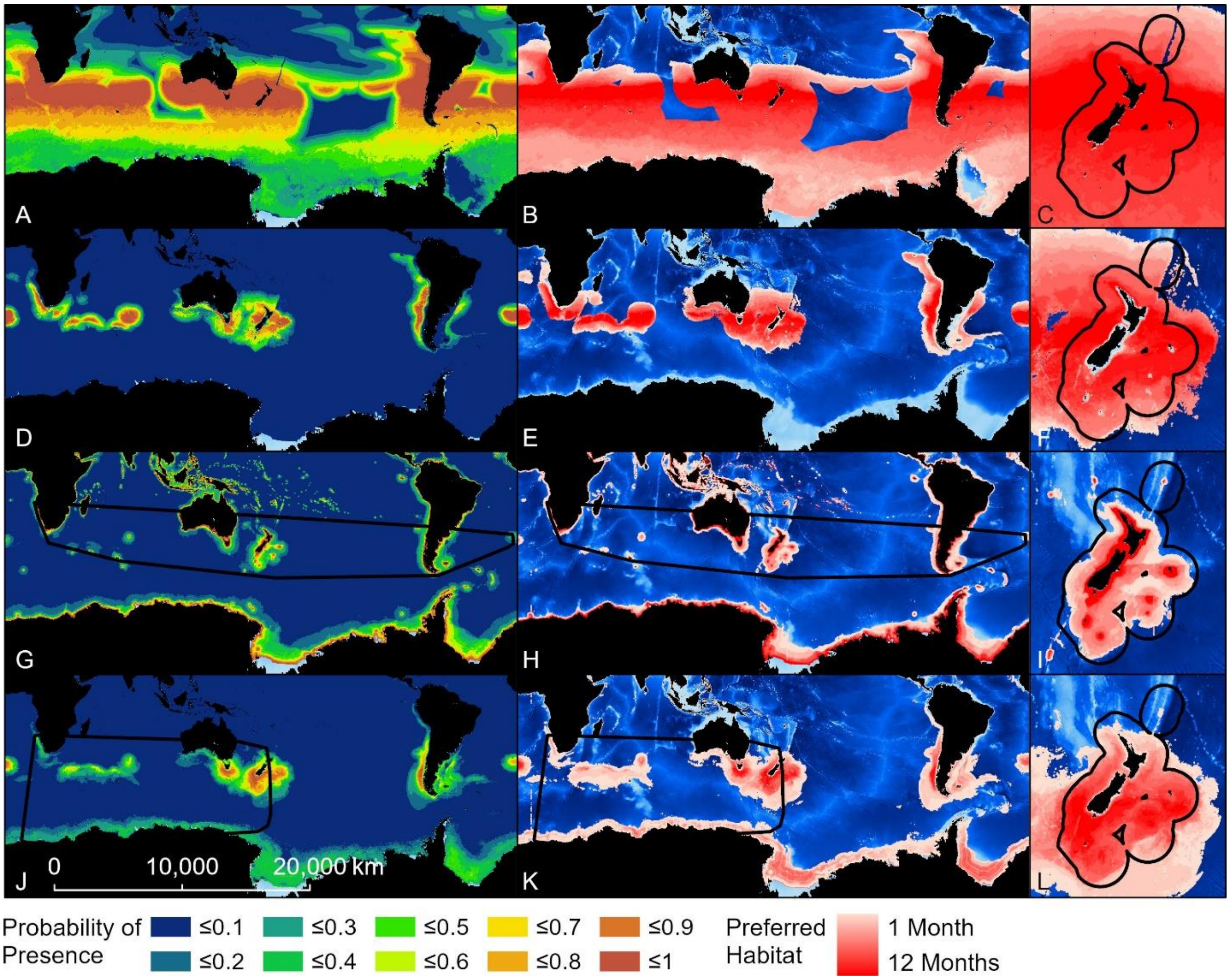

Supplementary Figure 14. Probability of presence and habitat of white-capped albatross predicted by four models. Top two rows show results from two Relative Environmental Suitability models (one fit with values obtained from the monthly 50% kernel density contours from geolocation data (RES_{KERN}, **A-C**), and one fit with values from the literature and expert opinion (RES_{LIT}, **D-F**)). Bottom two rows show results from two boosted regression tree models (one fit with opportunistic sightings data (BRT_{OS}, **G-I**), and one fit with geolocation data (BRT_{GL}, **J-L**)). Black boundaries indicate the minimum convex hull (**G, H, J, K**) or NZ Exclusive Economic Zone (**C, F, I, L**) and habitat is color-scaled from 1 to 12 indicating the number of months each cell was classified as habitat.

10 BRT model uncertainty

The following figures depict the uncertainty in the predicted probability of occurrence for boosted regression tree models. A spatial depiction of standard deviation was created for each month based on the results from 200 bootstraps for each BRT model, and then averaged across months to represent overall uncertainty in the mean probably of occurrence across months.

10.1 Campbell albatross

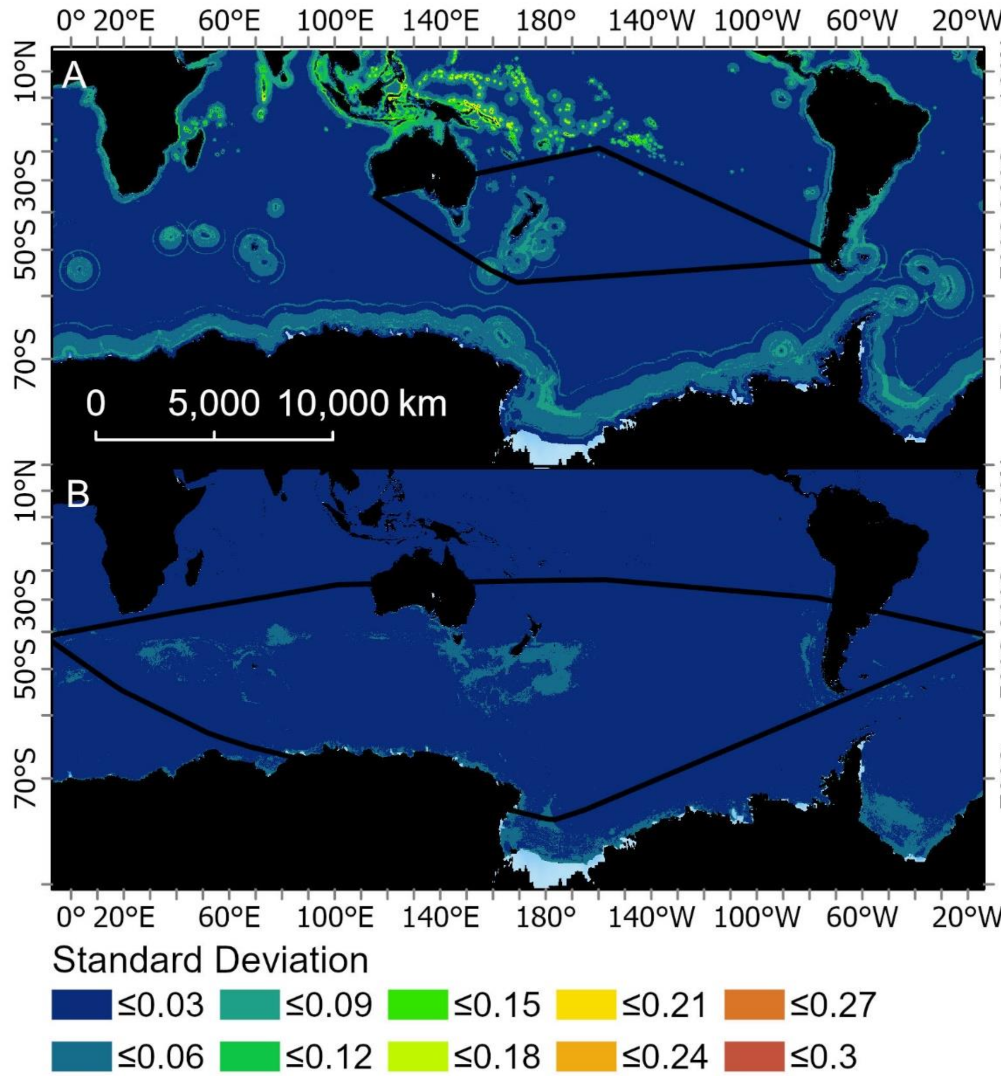

Supplementary Figure 15. Mean of the monthly standard deviations created from the 200 bootstraps for two boosted regression tree models used to predict the probably of occurrence for Campbell albatross (one fit with opportunistic sightings data (BRT_{OS}, **A**), and one fit with geolocation data (BRT_{GL}, **B**)). Black boundaries indicate the minimum convex hull around the data that were used to fit each respective BRT model.

10.2 Grey-headed albatross

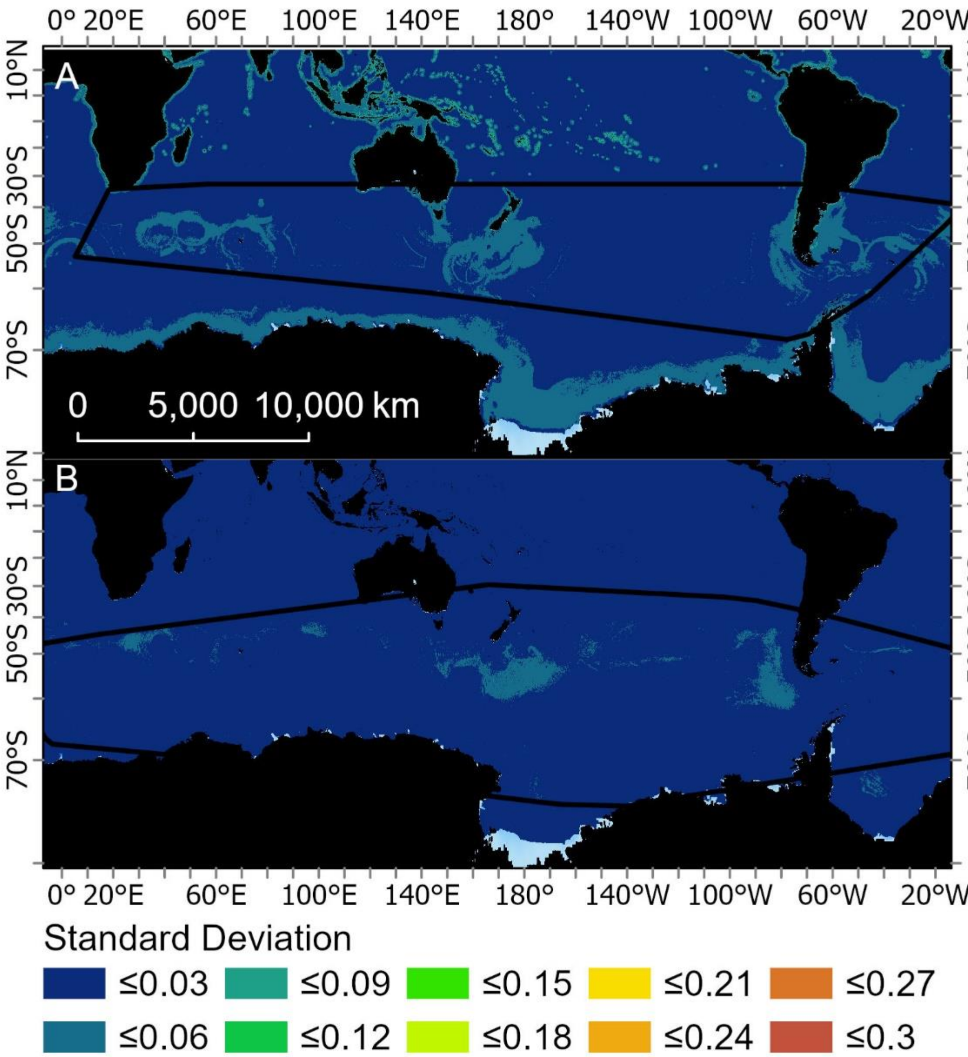

Supplementary Figure 16. Mean of the monthly standard deviations created from the 200 bootstraps for two boosted regression tree models used to predict the probably of occurrence for grey-headed albatross (one fit with opportunistic sightings data (BRT_{OS}, **A**), and one fit with geolocation data (BRT_{GL}, **B**)). Black boundaries indicate the minimum convex hull around the data that were used to fit each respective BRT model.

10.3 White-capped albatross

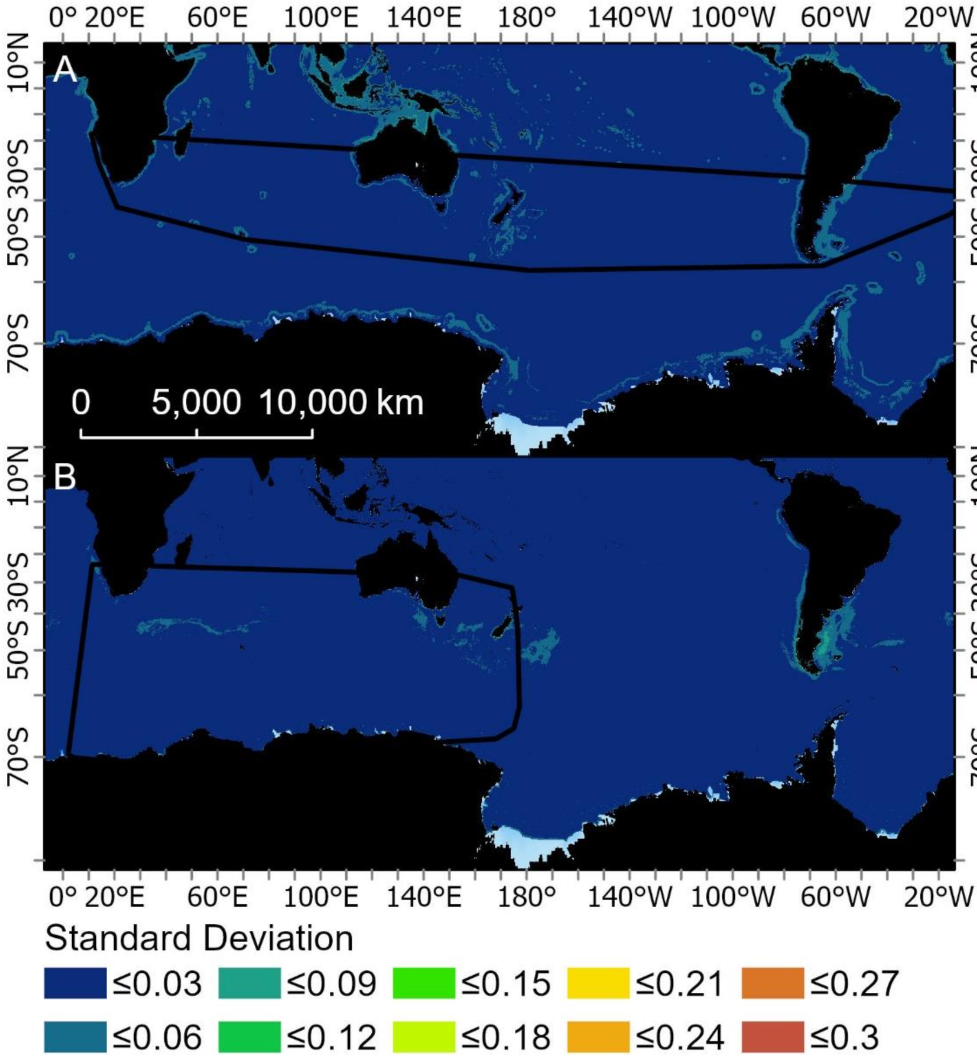

Supplementary Figure 17. Mean of the monthly standard deviations created from the 200 bootstraps for two boosted regression tree models used to predict the probably of occurrence for white-capped albatross (one fit with opportunistic sightings data (BRT_{OS}, **A**), and one fit with geolocation data (BRT_{GL}, **B**)). Black boundaries indicate the minimum convex hull around the data that were used to fit each respective BRT model.

11 Overlap with global fishing effort

The following figures depict the mean total fishing effort (hrs) (based on data from Global Fishing Watch) per month that occurs within the preferred habitat of Campbell, grey-headed, and white-capped albatross.

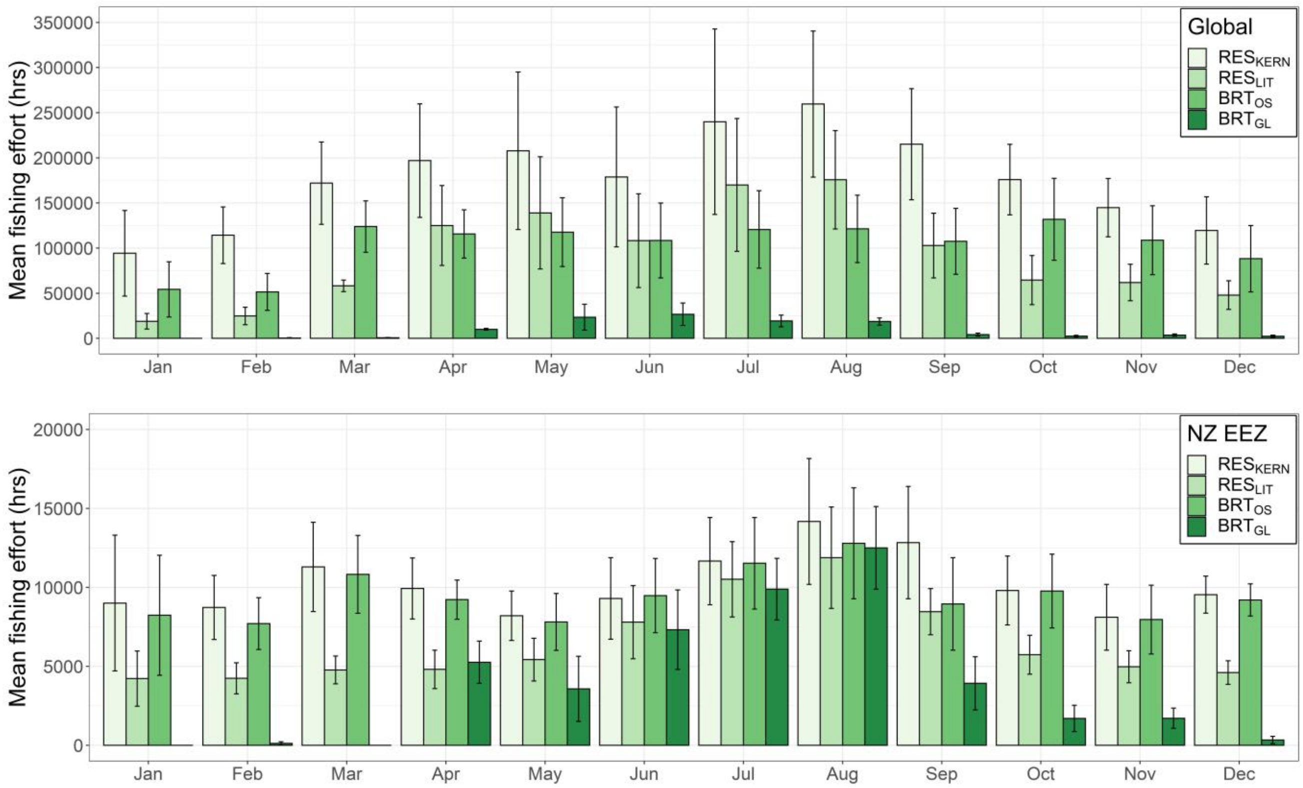

Supplementary Figure 18. Mean total fishing effort (hrs) (based on data from Global Fishing Watch) per month that occurs within the preferred habitat of Campbell albatross both globally (top) and within New Zealand's Exclusive Economic Zone (bottom). Colour coding denotes different habitat suitability models and error bars indicate one standard deviation.

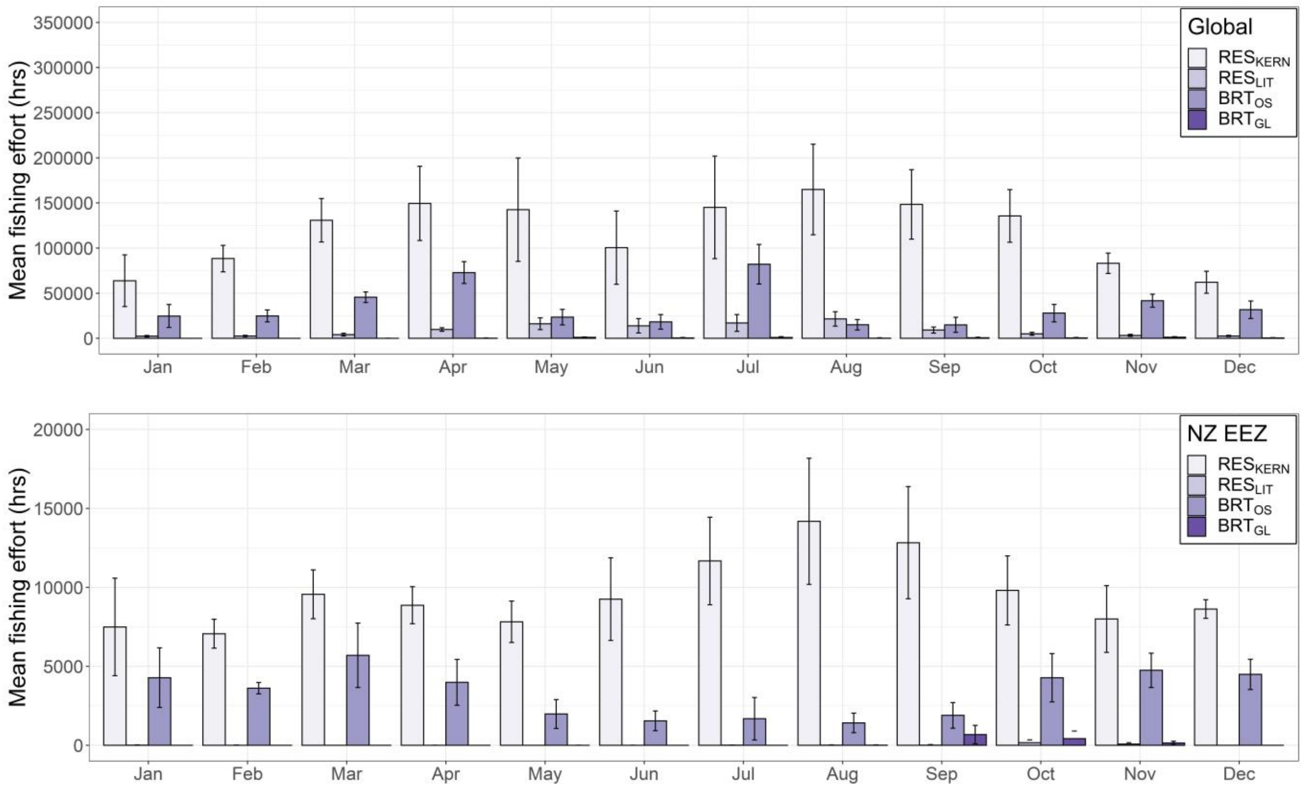

Supplementary Figure 19. Mean total fishing effort (hrs) (based on data from Global Fishing Watch) per month that occurs within the preferred habitat of grey-headed albatross both globally (top) and within New Zealand's Exclusive Economic Zone (bottom). Colour coding denotes different habitat suitability models and error bars indicate one standard deviation.

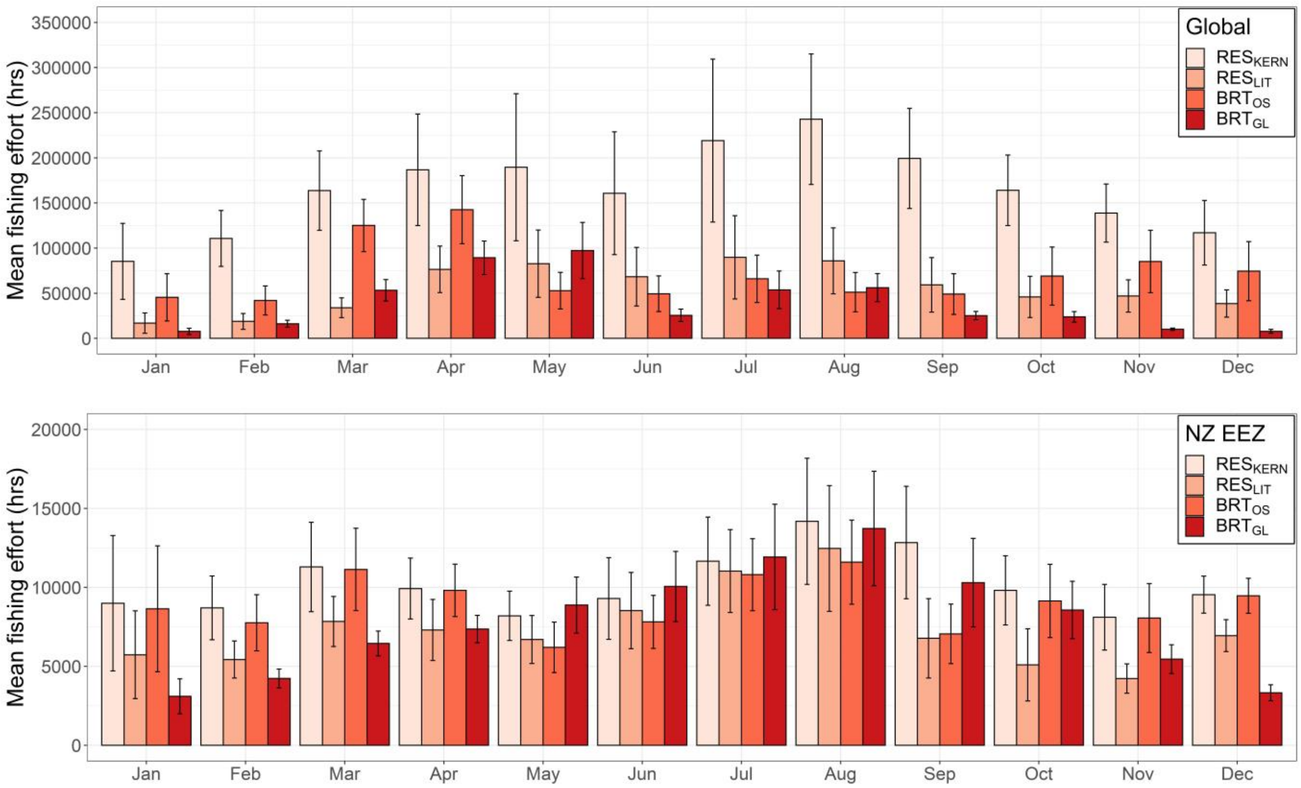

Supplementary Figure 20. Mean total fishing effort (hrs) (based on data from Global Fishing Watch) per month that occurs within the preferred habitat of white-capped albatross both globally (top) and within New Zealand's Exclusive Economic Zone (bottom). Colour coding denotes different habitat suitability models and error bars indicate one standard deviation.

12 Reference List

Amante, C., and Eakins, B. (2009). ETOPO1 1 Arc-Minute Global Relief Model: Procedures, data sources and analysis. *NOAA Technical Memorandum NESDIS NGDC-24***,** 19.

Casey, K.S., and Cornillon, P. (1999). A comparison of satellite and in situ–based sea surface temperature climatologies. *Journal of Climate* 12**,** 1848-1863.

Catry, P., Phillips, R.A., and Croxall, J.P. (2004). Sustained fast travel by a gray-headed albatross (*Thalassarche chrysostoma*) riding an Antarctic storm. *The Auk* 121**,** 1208-1213.

Cleeland, J.B., Alderman, R., Bindoff, A., Lea, M.-A., Mcmahon, C.R., Phillips, R.A., Raymond, B., Sumner, M.D., Terauds, A., and Wotherspoon, S. (2019). Factors influencing the habitat use of sympatric albatrosses from Macquarie Island, Australia. *Marine Ecology Progress Series* 609**,** 221-237.

Esri (2019). "ArcGIS Pro Version 2.4.1, Redlands, CA: Environmental Systems Research Institute".).

Kroeger, C., Crocker, D.E., Thompson, D.R., Torres, L.G., Sagar, P., and Shaffer, S.A. (2019). Variation in Corticosterone Levels in Two Species of Breeding Albatrosses with

Divergent Life Histories: Responses to Body Condition and Drivers of Foraging Behavior. *Physiological and Biochemical Zoology* 92**,** 223-238.
Louzao, M., Hyrenbach, K.D., Arcos, J.M., Abelló, P., De Sola, L.G., and Oro, D. (2006). Oceanographic habitat of an endangered Mediterranean procellariiform: implications for marine protected areas. *Ecological Applications* 16**,** 1683-1695.
Nasa Goddard Space Flight Center, Ocean Ecology Laboratory, and Ocean Biology Processing Group (2018). Moderate-resolution Imaging Spectroradiometer (MODIS) Aqua Chlorophyll Data. *2018 Reprocessing*.
Nel, D., Lutjeharms, J., Pakhomov, E., Ansorge, I., Ryan, P., and Klages, N. (2001). Exploitation of mesoscale oceanographic features by grey-headed albatross *Thalassarche chrysostoma* in the southern Indian Ocean. *Marine Ecology Progress Series* 217**,** 15-26.
Petersen, S.L., Phillips, R.A., Ryan, P.G., and Underhill, L.G. (2008). Albatross overlap with fisheries in the Benguela Upwelling System: implications for conservation and management. *Endangered Species Research* 5**,** 117-127.
Poupart, T.A., Waugh, S.M., Miskelly, C.M., Kato, A., Angel, L.P., Rogers, K.M., and Arnould, J.P. (2019). Fine-scale foraging behaviour of southern Buller's albatross, the only Thalassarche that provisions chicks through winter. *Marine Ecology Progress Series* 625**,** 163-179.
Sagar, P., and Weimerskirch, H. (1996). Satellite tracking of southern Buller's albatrosses from The Snares, New Zealand. *The Condor* 98**,** 649-652.
Scales, K.L., Miller, P.I., Ingram, S.N., Hazen, E.L., Bograd, S.J., and Phillips, R.A. (2016). Identifying predictable foraging habitats for a wide-ranging marine predator using ensemble ecological niche models. *Diversity and Distributions* 22**,** 212-224.
Spear, L.B., Ainley, D.G., and Webb, S.W. (2003). Distribution, abundance and behaviour of Buller's, Chatham Island and Salvin's Albatrosses off Chile and Peru. *Ibis* 145**,** 253-269.
Stahl, J., Bartle, J., Cheshire, N., Petyt, C., and Sagar, P. (1998). Distribution and movements of Buller's albatross (*Diomedea bulleri*) in Australasian seas. *New Zealand Journal of Zoology* 25**,** 109-137.
Stahl, J., and Sagar, P. (2000a). Foraging strategies and migration of southern Buller's albatrosses *Diomedea b. bulled* breeding on the Solander Is, New Zealand. *Journal of the Royal Society of New Zealand* 30**,** 319-334.
Stahl, J., and Sagar, P. (2000b). Foraging strategies of southern Buller's albatrosses *Diomedea b. bulleri* breeding on The Snares, New Zealand. *Journal of the Royal Society of New Zealand* 30**,** 299-318.
Stahl, J., and Sagar, P. (2006). Behaviour and patterns of attendance of non-breeding birds at the breeding colony in a Buller's albatross *Thalassarche bulleri* population at The Snares. *Notornis* 53**,** 327.
Sztukowski, L.A., Cotton, P.A., Weimerskirch, H., Thompson, D.R., Torres, L.G., Sagar, P.M., Knights, A.M., Fayet, A.L., and Votier, S.C. (2018). Sex differences in individual foraging site fidelity of Campbell albatross. *Marine Ecology Progress Series* 601**,** 227-238.
Sztukowski, L.A., Van Toor, M.L., Weimerskirch, H., Thompson, D.R., Torres, L.G., Sagar, P.M., Cotton, P.A., and Votier, S.C. (2017). Tracking reveals limited interactions between Campbell Albatross and fisheries during the breeding season. *Journal of Ornithology* 158**,** 725-735.

Torres, L.G., Smith, T.D., Sutton, P., Macdiarmid, A., Bannister, J., and Miyashita, T. (2013). From exploitation to conservation: habitat models using whaling data predict distribution patterns and threat exposure of an endangered whale. *Diversity and Distributions* 19**,** 1138-1152.

Torres, L.G., Thompson, D.R., Bearhop, S., Votier, S., Taylor, G.A., Sagar, P.M., and Robertson, B.C. (2011). White-capped albatrosses alter fine-scale foraging behavior patterns when associated with fishing vessels. *Marine Ecology Progress Series* 428**,** 289-301.

Wakefield, E.D., Phillips, R.A., Trathan, P.N., Arata, J., Gales, R., Huin, N., Robertson, G., Waugh, S.M., Weimerskirch, H., and Matthiopoulos, J. (2011). Habitat preference, accessibility, and competition limit the global distribution of breeding Black-browed Albatrosses. *Ecological Monographs* 81**,** 141-167.

Watson, H., Hiddink, J.G., Hobbs, M.J., Brereton, T.M., and Tetley, M.J. (2013). The utility of relative environmental suitability (RES) modelling for predicting distributions of seabirds in the North Atlantic. *Marine Ecology Progress Series* 485**,** 259-273.

Waugh, S., Weimerskirch, H., Cherel, Y., Shankar, U., Prince, P., and Sagar, P. (1999). Exploitation of the marine environment by two sympatric albatrosses in the Pacific Southern Ocean. *Marine Ecology Progress Series* 177**,** 243-254.

Wessel, P., and Smith, W.H.F. (1996). A global, self-consistent, hierarchical, high-resolution shoreline database. *Journal of Geophysical Research: Solid Earth* 101**,** 8741-8743.